Structural and Thermodynamic Aspects of the Interaction between Heparan Sulfate and Analogues of Melittin†

Elisabete Gonçalves,‡ Eric Kitas,§ and Joachim Seelig*,‡

Division of Biophysical Chemistry, Biozentrum, University of Basel, Klingelbergstrasse 70, CH-4056 Basel, Switzerland, and Pharma Division, Preclinical Research, F. Hoffmann-La Roche Ltd., CH-4070 Basel, Switzerland

Received November 1, 2005; Revised Manuscript Received December 22, 2005

ABSTRACT: Melittin is an amphipathic cationic peptide derived from honeybee venom with well-known cytolytic and antimicrobial properties. When coupled to cationic polymers or lipid molecules, it forms conjugates with high transfection efficiency and low toxicity with promising applications in gene therapy. A first step in the internalization of melittin and its conjugates is their binding to the cell surface, a reaction likely to involve heparan sulfate proteoglycans (HSPG). In the present work, we characterize the binding equilibrium of heparan sulfate (HS) with two melittin analogues, [Cys^1]melittin (mel-SH) and retro-inverso [Cys^1]melittin (ri-mel-SH). The terminal cysteine found in these peptides replaces the N-terminal glycine present in native melittin and allows covalent binding to other molecules. Isothermal titration calorimetry (ITC) reveals a high affinity of each melittin analogue to HS. Association constants of 4.7×10^4 and 3.5×10^5 M^{-1} are found at physiological ionic strength and 15 °C for ri-mel-SH and mel-SH, respectively. The reaction enthalpy measured under these conditions is $\Delta H^\circ_{pep} = 4.2$ kcal/mol for ri-mel-SH and $\Delta H^\circ_{pep} = 1.1$ kcal/mol for mel-SH. The peptide-to-HS stoichiometry is ∼20 for ri-mel-SH and ∼14 for mel-SH under the same conditions. Temperature dependence studies using ri-mel-SH (mel-SH) show that ΔH°_{pep} decreases in magnitude upon increase in temperature, which results in a molar heat capacity of $\Delta H^\circ_{pep} = -322$ cal mol^{-1} K^{-1} (-45 cal mol^{-1} K^{-1}). Such a negative heat capacity change is not expected for a purely electrostatic interaction and indicates that hydrophobic and other interactions are also involved in the binding equilibrium. Salt dependence studies of the binding constants confirm that nonelectrostatic forces are an important component of the HS-melittin interaction. Binding to HS induces conformational changes in both peptides, with ri-mel-SH showing a 6-fold increase of the α-helix content when incubated with HS under saturation conditions.

Melittin, the major component of honeybee venom from *Apis melifera*, is a 26-residue amphipathic peptide with well-known cytolytic and antimicrobial properties (*1*, *2*). Its water solubility and yet strong affinity to lipid membranes along with interesting conformational properties make it one of the best characterized antimicrobial peptides (for recent reviews cf. *3*−*5*). Largely unstructured in water, melittin readily folds into an amphipathic α-helix upon binding to lipid membranes, where it inserts and causes major disturbances such as pore formation and membrane solubilization (*6*, *7* and references therein). Due to the extreme sensitivity of melittin to the surrounding environment, it can also adopt a variety of conformation and aggregation states in aqueous solution. For instance, while monomeric and mostly random coil at low ionic strength and low peptide concentration, melittin aggregates into a tetramer with pronounced helical structure when the salt and/or peptide concentrations are increased (*8*−*10*).

The membrane-disturbing properties of melittin combined with the net positive charge (+5 to +6) make this peptide an interesting candidate for gene delivery. However, because melittin is also highly hemolytic (*2*, *11*, *12*), its therapeutic applications are largely dependent on the development of nonhemolytic analogues. Several strategies have been developed to overcome the toxic effects of melittin while keeping its potential therapeutic activity (*13*−*16*). One such strategy consists of conjugating melittin to polyethylenimine (PEI), a cationic polymer commonly used in gene transfection (*17*, *18*). The resulting melittin−PEI conjugates are nonhemolytic, form stable complexes with DNA, and increase gene transfection up to 3 orders of magnitude when compared to unconjugated PEI (*16*, *19*, *20*). The enhanced gene transfer correlates with an improved endosomal release, which is attributed to the ability of melittin to disrupt the endosome membrane and thereby facilitate DNA release into the cytoplasm (*16*, *20*).

Another example of a hybrid molecule with improved transfection efficiency and reduced toxicity is dioleoylmelittin. Formed by covalently coupling melittin to a derivative of dioleoylphosphatidylethanolamine (DOPE), this melittin-lipid conjugate binds DNA via the cationic peptide and forms complexes that produce high levels of gene expression even in the presence of serum (*14*). While the exact transfection mechanism of dioleoylmelittin is still unresolved, it is likely that, similarly to melittin−PEI conjugates, melittin-induced endosome rupture is involved (*14*).

† This work was supported by the Swiss National Foundation (Grant No. 31.58800.99).

* To whom correspondence should be addressed. Tel: +41-61-267 2190. Fax: +41-61-267 2193. E-mail: Joachim.seelig@unibas.ch.

‡ University of Basel.

§ F. Hoffmann-La Roche Ltd.

10.1021/bi052221t CCC: $33.50
Published on Web 02/09/2006

A first step in gene transfection is the binding of DNA complexes to the cell surface (*21*). Recent studies show that heparan sulfate proteoglycans (HSPG), a group of sulfated glycoproteins found in the extracellular matrix and at the surface of eukaryotic cells (*22, 23*), are receptors for cationic lipid−DNA complexes (*24, 25*). These polyanionic molecules have also been implicated in the internalization of several cell-penetrating peptides, including the full Tat protein (*26, 27*) and the oligoarginine R_9 (*28*). In both cases, the cationic moiety of the molecule interacts electrostatically with the anionic groups of heparan sulfate (HS)[1] (*25, 29, 30*), the sulfated polysaccharides present in HSPG (*22, 23*).

The net positive charge of melittin and of its conjugates suggests that, similarly to cationic lipids and cell-penetrating peptides, the cellular uptake of these molecules is mediated by HSPG. The cationic residues of melittin should provide strong affinity to the polyanionic HS chains, thereby strengthening the binding of this peptide to the cell plasma membrane. Although numerous studies have explored the interaction of melittin with lipid membranes (*7, 31*−*34*), no study has, to our knowledge, addressed its potential interaction with HS. The main goal of the present work is to address this issue by studying the binding equilibrium of HS with two melittin analogues, [Cys[1]]melittin (mel-SH) and retro-inverso [Cys[1]]melittin (ri-mel-SH). These peptides can be covalently linked to other molecules via the terminal cysteine, which replaces the N-terminal glycine found in native melittin. Mel-SH is the intermediate used to synthesize melittin-PEI and dioleoylmelittin, the two melittin conjugates mentioned above. The retro-inverso analogue, ri-mel-SH, has the reversed peptide amino acid sequence of mel-SH and is composed of all-D amino acids. As a retro-inverso peptide, it should show higher resistance to proteolytic degradation and have an improved bioavailability when compared to mel-SH (*35, 36*), thus leading to melittin conjugates with potentially better in vivo gene transfection performance.

Isothermal titration calorimetry (ITC), a high-sensitivity calorimetric technique capable of providing the full thermodynamic characterization of a binding event (*37*), was used to measure the thermodynamic parameters of the interaction between HS and the two melittin analogues. In parallel, structural changes in the peptides induced by HS binding were followed by circular dichroism (CD) spectroscopy.

MATERIALS AND METHODS

Materials. Heparan sulfate (HS), fraction I, sodium salt (from porcine intestinal mucosa, average MW 14200 Da, sulfur content 6.44%), was purchased from Celsus Laboratories (Cincinnati, OH). The two melittin analogues, [Cys[1]]-melittin (mel-SH) and the retro-inverso [Cys[1]]melittin (ri-mel-SH), were prepared using standard Fmoc-solid-phase peptide synthesis (*38*). All other chemicals were of analytical or reagent grade. Tris buffer (10 mM tris(hydroxymethyl)-aminoethane, pH 7.4) was prepared from 18 MΩ water obtained from a NANOpure A filtration system. NaCl concentrations were variable (25 to 350 mM) and are specified in the legends of each figure. Synthetic melittin was obtained from Bachem (Bubendorf, Switzerland).

Isothermal Titration Calorimetry. All measurements were made with a MicroCal VP-ITC calorimeter (MicroCal, Northampton, MA). To avoid air bubbles, all solutions were degassed under vacuum prior to use. Typically, ri-mel-SH titrations were performed by injecting 4 μL aliquots of HS (200 μM) into the calorimeter cell (V_{cell} = 1.4037 mL) containing ri-mel-SH (100 μM), at constant time intervals of 7 min. For the mel-SH titrations, the peptide concentration in the calorimeter cell was typically 200 μM, and 8 μL aliquots of 200 μM HS were injected every 6 min. To minimize the error associated with diffusion from the syringe during baseline equilibration, the volume of HS injected in the first injection was smaller than the remaining injections (1.5−2.5 μL), and the associated heat was not included in the data analysis. Heats of dilution (∼1−2 μcal) were measured in control titrations, in which HS was titrated into pure buffer, and were included in the final analysis. Raw data were processed using Origin graphing software provided with the instrument. The temperature was set as indicated in the legend of the figures.

Binding Model. The binding data were evaluated according to a multisite binding model. Used successfully to describe the binding equilibria of other peptides to HS (*29, 30, 39*), this model is represented by the following equation (*40, 41*)

$$\frac{[P]_b}{[HS]_t} = \frac{nK[P]}{1 + K[P]} \quad (1)$$

where [P] and $[P]_b$ are the concentration of free and bound peptide, respectively, $[HS]_t$ is the total concentration of heparan sulfate, K is the intrinsic binding constant, and n is the number of peptide molecules bound per HS polysaccharide chain. Due to mass conservation, the concentration of bound peptide is described by

$$[P]_b = \frac{1}{2}\left(\frac{1}{K} + [P]_t + n[HS]_t\right) - \frac{1}{2}\sqrt{\left(\frac{1}{K} + [P]_t + n[HS]_t\right)^2 - 4n[HS]_t[P]_t} \quad (2)$$

with $[P]_t$ denoting the total peptide concentration. Because the heat associated with the binding event is proportional to the concentration of bound peptide, $[P]_b$, the heat absorbed (or released) in injection i, δQ_i, is given by

$$\delta Q_i = \Delta H^\circ_{pep} \delta[P]_{b,i} V \quad (3)$$

where ΔH°_{pep} is the peptide binding enthalpy, $\delta[P]_{b,i}$ is the change (increase) in bound peptide concentration upon injection i, and V is the reaction volume (including dilution effects) (*37*).

Circular Dichroism Spectroscopy. All measurements were carried out at room temperature using a JASCO J720 spectropolarimeter (Japan-Spectroscopic, Tokyo, Japan). A quartz cell with a path length of 0.1 cm was used, and all spectra were corrected by subtracting the buffer baseline. A 200 μM stock solution of each melittin analogue was prepared in Tris buffer (10 mM Tris, 100 mM NaF, pH 7.4) and diluted to the appropriate peptide concentration, either in the absence or presence of HS. Results are reported as

[1] Abbreviations: mel-SH, [Cys[1]]melittin; ri-mel-SH, retro-inverso [Cys[1]]melittin; HS, heparan sulfate; HSPG, heparan sulfate proteoglycans; ITC, isothermal titration calorimetry; CPPs, cell-penetrating peptides; CD, circular dichroism spectroscopy.

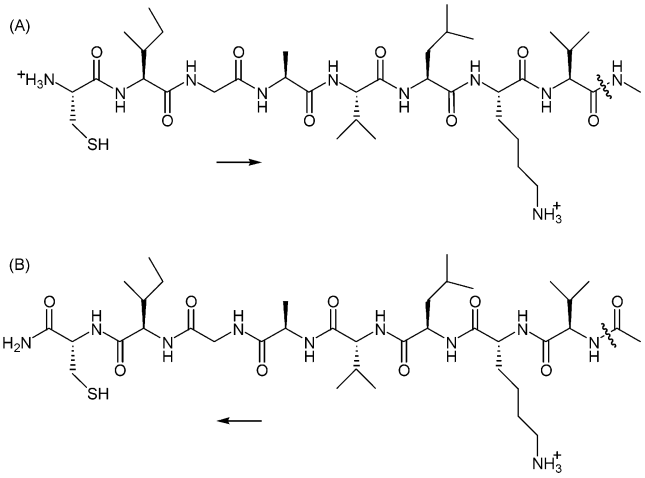

FIGURE 1: Schematic representation of the analogues of melittin used in this study: (A) **CIGAVLKV**LTTGLPALISWIKRKRQQ-NH_2 (mel-SH) and (B) qqrkrkiwsilaplGttl**vklvaGic-NH_2** (ri-mel-SH). Only the portion of the amino acid sequences that is highlighted in bold is schematically shown. Although the amide bonds run in opposite directions (indicated by the arrows), the orientation of the side chains is similar in both peptide structures.

mean residue ellipticity in units of deg cm^2 $dmol^{-1}$. The percentage of peptide secondary structure was estimated from a computer simulation based on the reference CD spectra obtained by Reed and Reed (*42*).

RESULTS

Melittin Analogues. The analogues of melittin used in the present study are schematically represented in Figure 1, where part of their chemical structure is shown. Mel-SH (Figure 1A) has the same amino acid sequence as bee melittin, with the difference that the glycine found in the N-terminus of melittin is replaced by a cysteine in mel-SH. In the retro-inverso analogue of mel-SH (Figure 1B), the L-amino acid residues have been replaced by the corresponding D-isomers, and the peptide amino acid sequence is reversed. As a consequence, while both peptides display an identical orientation of their side chains, the peptide backbone direction of ri-mel-SH is reversed due to the replacement of the natural peptide bond ψ(CO-NH) with ψ(NH-CO) bonds.

Binding of HS to ri-mel-SH. The interaction of ri-mel-SH with HS was studied by isothermal titration calorimetry. Figure 2 shows a representative calorimetric trace (Figure 2A) and the corresponding titration curve (Figure 2B) obtained at 15 °C by titration of ri-mel-SH (100 μM) with 4 μL aliquots of HS (200 μM). The integrated heats in Figure 2B represent the net heats of each injection after subtracting the dilution heats of HS into pure buffer. The upward direction of the titration peaks (Figure 2A) and the corresponding positive integrated heats (Figure 2B) indicate that binding of ri-mel-SH to HS is an endothermic reaction. The heats measured in the first few injections are relatively constant (~79 μcal) but become progressively smaller as the titration proceeds and the concentration of free ri-mel-SH decreases. Ultimately, all available peptide is bound to HS, and the small heats measured in the last few injections are due to the dilution of HS into buffer. Under such conditions, an estimate of the peptide molar binding enthalpy, ΔH°_{pep}, may be obtained by dividing the total heat absorbed in the titration (~1075 μcal) by the total amount of ri-mel-SH in the calorimeter cell (140.4 nmol) (*43*, *44*). Following this simple approach, a $\Delta H^\circ_{pep} = 7.7$ kcal/mol (at 15 °C, 50 mM NaCl, 10 mM Tris, pH 7.4) is determined from Figure 2B. The HS binding enthalpy, ΔH°_{HS}, can also be estimated from Figure 2B by assuming that in the beginning of the titration the injected HS is immediately and completely saturated with ri-mel-SH (*43*, *44*). As the amount of injected HS is 0.8 nmol and the measured heat per injection is 79 μcal, this leads to a $\Delta H^\circ_{HS} = 98.8$. Consequently, the total number of ri-mel-SH molecules bound to one HS molecule is $n = \Delta H^\circ_{HS}/\Delta H^\circ_{pep} = 98.8/7.7 = 12.9$.

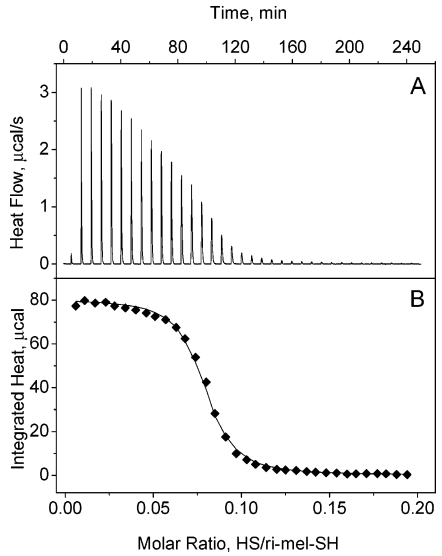

FIGURE 2: Titration of HS into ri-mel-SH. (A) Calorimetric trace obtained at 15 °C by titration of HS (200 μM) into a solution of ri-mel-SH (100 μM). Each peak corresponds to the injection (at 7 min intervals) of 4 μL of HS into the calorimeter cell ($V = 1.4037$ mL), except for the first peak where only 2 μL was injected. (B) Heats of reaction (integrated from the calorimetric trace) plotted as a function of the HS/ri-mel-SH molar ratio. The solid line is the best fit to the experimental data (◆) using the binding model described by eqs 1−3 (cf. Table 1 for parameters). Buffer: 10 mM Tris, 50 mM NaCl, pH 7.4.

For a complete thermodynamic characterization of the binding isotherm, the calorimetric data has to be treated with an appropriate binding model. A long polymer such as HS (MW ~14200 Da) may be described as a macromolecule with *n* independent and equivalent binding sites for a ligand like ri-mel-SH (for details regarding the binding model, see Materials and Methods). The solid line in Figure 2B is the best least-squares fit to the data using eqs 1−3 yielding the following set of parameters: $n = 12.9$, $K = 8.0 \times 10^5$ M^{-1}, and $\Delta H^\circ_{pep} = 7.8$ kcal/mol (cf. Table 1). The *n* and ΔH°_{pep} parameters derived with this model are consistent with the direct evaluation discussed above.

Table 1 summarizes the thermodynamic parameters obtained at various temperatures using the binding model described by eqs 1−3. ΔH°_{pep} is positive at all temperatures tested, decreasing from ~11 kcal/mol to ~2 kcal/mol as the temperature is raised from 5 to 35 °C. From the slope of the straight line shown in Figure 3A, we obtain a negative heat capacity change of $\Delta H^\circ_p = -322$ cal mol^{-1} K^{-1}. Further inspection of Table 1 reveals that the reaction is entropy-driven, as indicated by the positive $T\Delta S^\circ_{pep}$ values, and that the affinity of HS to ri-mel-SH increases upon increase in temperature, as indicated by larger *K* values. The solid line

Table 1: Thermodynamic Parameters for ri-mel-SH Binding to Heparan Sulfate[a]

T (°C)	binding stoichiometry (n)	K (M^{-1})	ΔH°_{pep} (kcal/mol)	ΔG°_{pep} (kcal/mol)	$T\Delta S^\circ_{pep}$ (kcal/mol)
5	13.0 ± 0.0	$(3.5 \pm 0.7) \times 10^5$	11.0 ± 0.1	-7.1 ± 0.1	18.0 ± 0.1
15	12.9 ± 0.1	$(6.5 \pm 0.7) \times 10^5$	7.8 ± 0.1	-7.7 ± 0.1	15.4 ± 0.1
25	15.7 ± 1.5	$(7.8 \pm 0.8) \times 10^5$	3.4 ± 0.7	-8.0 ± 0.1	11.3 ± 0.5
35	13.0 ± 1.4	$(9.4 \pm 0.5) \times 10^5$	1.7 ± 0.2	-8.4 ± 0.1	10.1 ± 0.1

[a] Data represent the average ± standard deviation of three measurements. Buffer: 10 mM Tris and 50 mM NaCl at pH 7.4.

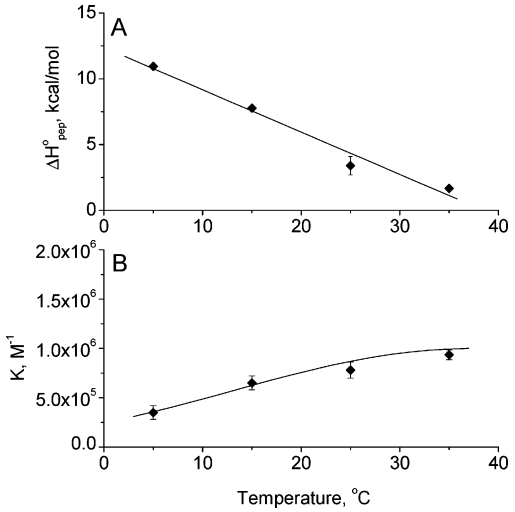

FIGURE 3: Temperature dependence of the reaction enthalpy, ΔH°_{pep}, (A) and the binding constant, K, (B) for ri-mel-SH binding to heparan sulfate. Linear regression analysis of the experimental data in (A) yields ΔH°_{pep} (kcal/mol) = 12.39 − 0.322T(°C) (solid line). The solid line in (B) is the predicted temperature dependence of K using the above regression formula for $\Delta H^\circ_{pep}(T)$. Buffer: 10 mM Tris, 50 mM NaCl, pH 7.4.

in Figure 3B describes the predicted temperature dependence of K based on the van't Hoff relation, $d \ln K/dT = \Delta H^\circ_{pep}/RT^2$, and taking into account the temperature-dependence of ΔH°_{pep} (Figure 3A). Within the accuracy of the measurements, a good agreement between experimental data and theory is obtained. The binding stoichiometry is independent of temperature with $n = 13.5 \pm 1.5$ (50 mM NaCl, 10 mM Tris, pH 7.4).

Binding of HS to mel-SH. At high salt concentrations (250 and 350 mM NaCl, 15 °C), the calorimetric titration of mel-SH with HS shows the same qualitative appearance as in Figure 2. The analysis in terms of eqs 1−3, assuming n identical and independent binding sites, yields the thermodynamic parameters listed in Table 2. At lower salt concentrations, the ITC data exhibit a more complex behavior. The titration of mel-SH with HS in 150 mM NaCl at 15 °C is shown in Figure 4 and indicates two stages of interactions. For the first five injections of HS (200 μM) into mel-SH (200 μM), the heats of reaction are fairly constant. The theoretical curve (solid line calculated with $n = 14.3$, $K = 3.0 \times 10^5$ M^{-1}, and $\Delta H^\circ_{pep} = 1.35$ kcal/mol) indicates that after five injections ~36% of the total mel-SH in the calorimeter cell is bound to HS. At this point, an additional endothermic reaction takes place, which extends between 36% and 77% of bound mel-SH. The additional heat, referenced to the total amount of mel-SH, is $\Delta H \approx 0.4$ kcal/mol, which is ~30% of the heat of binding reaction proper. The molecular nature of this second reaction is unclear at present. A similar phenomenon has been observed for the titration of DNA with multivalent cations and has been interpreted in terms of DNA condensation and aggregation (*45*). By analogy, the second stage in the HS-mel-SH interaction could correspond to a reorganization of the complex to a more compact aggregate.

At 50 mM NaCl, mel-SH binds to HS with approximately the same binding constant ($K = 6.3 \times 10^5$ M^{-1}) and stoichiometry ($n = 12$) as ri-mel-SH. However, the molar heat capacity change is reduced to $\Delta C^\circ_p = -45$ cal mol^{-1} K^{-1}.

The Effect of NaCl on the Interaction between HS and Melittin Analogues. The interaction between HS and melittin analogues was further characterized by analyzing the effect of NaCl on the binding equilibrium. To this purpose, both ri-mel-SH and mel-SH were titrated with HS at various NaCl concentrations. The thermodynamic parameters obtained at 15 °C with the binding model described by eq 1−3 are listed in Table 2. As anticipated for an electrostatic interaction, the binding affinity of HS to both melittin analogues decreases with increasing NaCl concentration. ΔH°_{pep} and $T\Delta S^\circ_{pep}$ also decrease in magnitude, but this decrease is more significant for the latter parameter. As the reaction enthalpy is endothermic for both peptides at all salt concentrations, the binding affinity, ΔG°_{pep}, is exclusively entropic in origin. As a control, we have included in Table 2 a titration with unmodified melittin in which the C-terminal amino acid is glycine instead of cysteine. The thermodynamic data are consistent with those obtained for mel-SH.

The contribution of electrostatics to the interaction of HS with melittin analogues can be determined by analyzing the salt dependence of the binding constant according to the theory of protein-polyelectrolyte interactions (*46*−*48*), with the assumption that HS behaves as a polyelectrolyte in solution. This analysis has been used to quantify the electrostatic and nonelectrostatic components of the interaction of various macromolecules with polyelectrolytes such as DNA (*49*, *50*) and heparin (*51*−*55*). According to this theory (*46*, *47*), when a peptide (P) binds to a linear polyelectrolyte (HS) to form a complex (HS·P_n), the counterions (M^+) condensed to the polyelectrolyte surface are released into bulk solution following the reaction:

$$HS(z_{M^+}\,M^+) + nP^{z+} \overset{K_T}{\rightleftharpoons} HS{\cdot}P_n + z_{M^+}M^+ \qquad (4)$$

Here, z_{M^+} is the number of counterions bound to free HS that are released into solution upon peptide binding; $z_{M^+} = z\psi$, where z is the number of purely ionic interactions formed between HS and the peptide, and ψ is the fraction of counterions bound to HS per unit charge. Since counterions enter the reaction with a stoichiometric coefficient z_{M^+}, the

Table 2: Effect of NaCl on the Thermodynamic Parameters of Heparan Sulfate Binding to Melittin Analogues at 15 °C[a]

NaCl (mM)	binding stoichiometry	K (M^{-1})	ΔH°_{pep} (kcal/mol)	ΔG°_{pep} (kcal/mol)	$T\Delta S^{\circ}_{pep}$ (kcal/mol)
unmodified melittin					
100	10.5 ± 1	$(4.9 \pm 0.5) \times 10^5$	1.9 ± 0.1	−7.5 ± 0.1	9.3 ± 0.2
mel-SH					
50	12.0 ± 1.4	$(6.3 \pm 1.1) \times 10^5$	1.4 ± 0.1	−7.6 ± 0.1	9.0 ± 0.2
100	12.5 ± 0.7	$(5.8 \pm 1.8) \times 10^5$	1.1 ± 0.2	−7.6 ± 0.2	8.6 ± 0.1
100[b]	14 ± 1.5	7.0×10^5	0.80 ± 0.1	−8.0	8.8
150	14.3 ± 0.1	$(3.5 \pm 0.7) \times 10^5$	1.1 ± 0.3	−7.3 ± 0.1	8.4 ± 0.2
250	17.1 ± 0.1	$(2.8 \pm 0.4) \times 10^5$	0.9 ± 0.2	−7.2 ± 0.1	8.1 ± 0.2
350	17.0 ± 1.4	$(1.4 \pm 0.1) \times 10^5$	0.8 ± 0.1	−6.8 ± 0.1	7.6 ± 0.1
ri-mel-SH					
25	14.8 ± 0.6	$(3.1 \pm 0.1) \times 10^6$	6.9 ± 0.1	−8.6 ± 0.1	15.5 ± 0.1
50	12.9 ± 0.1	$(6.5 \pm 0.7) \times 10^5$	7.8± 0.1	−7.7 ± 0.1	15.4 ± 0.1
100	12.8 ± 2.3	$(1.9 \pm 0.4) \times 10^5$	7.7 ± 1.5	−7.0 ± 0.1	14.6 ± 1.6
150	20.0 ± 0.0	$(4.7 \pm 1.1) \times 10^4$	4.2 ± 0.2	−6.2 ± 0.1	10.3 ± 0.1
350	24.0 ± 2.8	$(1.7 \pm 0.1) \times 10^4$	3.0 ± 1.8	−5.6 ± 0.1	8.6 ± 1.8

[a] Data represent the average ± standard deviation of two to three measurements. Buffer: 10 mM Tris and variable concentrations of NaCl at pH 7.4. [b] Measurement at 28 °C.

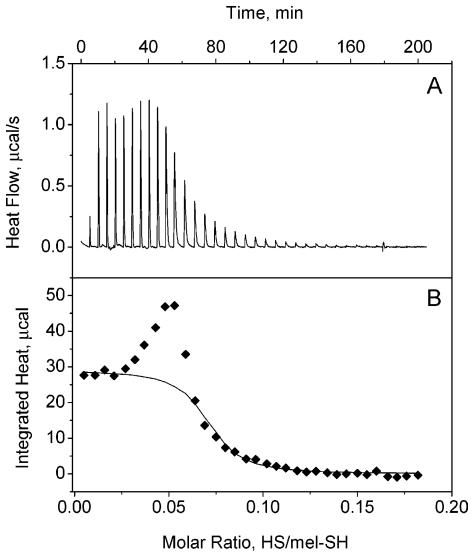

FIGURE 4: Titration of HS into mel-SH. (A) Calorimetric trace obtained at 15 °C by titration of HS (200 μM) into mel-SH (200 μM). Each peak corresponds to the injection (every 6 min) of 7.5 μL of HS into the calorimeter cell (V = 1.4037 mL), except for the first peak where only 2.5 μL was injected. (B) Heats of reaction (integrated from the calorimetric trace) plotted as a function of the HS/mel-SH molar ratio. The solid line is the best fit to the experimental data (◆) using the binding model described by eqs 1−3 with the parameters listed in Table 2. Buffer: 10 mM Tris, 150 mM NaCl, pH 7.4.

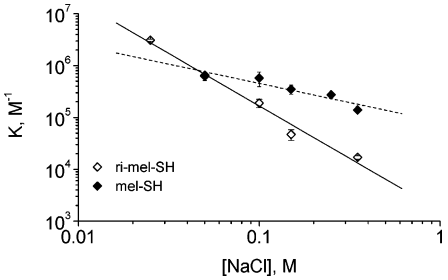

FIGURE 5: Salt dependence of the interaction between HS and melittin analogues. Binding constants (K) for HS binding to ri-mel-SH (◇) and mel-SH (◆) were determined as a function of NaCl concentration in Tris buffer (10 mM Tris, pH 7.4) from ITC measurements at 15 °C, as described in the legends of Figures 2 and 4. K values are plotted as a function of the NaCl concentration on a log/log scale. Linear regression analysis of the ri-mel-SH data (◇) yields log K = 3.20−2.02 log[NaCl] (solid line). For mel-SH (◆), the regressed line (dashed line) is described by log K = 4.92−0.74 log[NaCl].

overall total equilibrium constant K_T is described by

$$K_T = \frac{[HS{\cdot}P_n][M^+]^{z_{M+}}}{[HS][P]^n} = K[M^+]^{z_{M+}} \quad (5)$$

where K is the observed binding constant as normally defined (independent of buffer components). Taking the logarithm of both sides of eq 5 and rearranging gives

$$\log K = \log K_T - z_{M^+} \log M^+ \quad (6)$$

A plot of log K versus log [M^+] should thus be linear, with a slope equal to $-z_{M^+}$ and a y-intercept equal to log K_T. According to the polyelectrolyte theory, the slope of this straight line provides the number of purely ionic interactions involved in the association reaction, while the y-intercept at 1 M NaCl gives an estimate of the nonionic binding constant, K_T, which is equivalent to K minus electrostatic effects (*46*, *47*).

As predicted from eq 6, the observed binding constants of HS to each melittin analogue are linearly related to the NaCl concentration when plotted in a double-logarithmic axis (Figure 5). Regression analysis of the experimental data yields straight lines with slopes of −0.74 and −2.02 for mel-SH (dashed line) and ri-mel-SH (solid line), respectively, suggesting that between one and two Na^+ ions are released when melittin analogues bind to HS. The y-intercepts (log K_T) of the regressed lines are 3.20 for ri-mel-SH and 4.92 for mel-SH. The corresponding energy contributions will be discussed below.

Structural Aspects of the Interaction between HS and Melittin Analogues. To check for structural changes in mel-SH and ri-mel-SH induced by HS binding, we analyzed the secondary structure of each peptide in the absence and presence of HS with circular dichroism spectroscopy (Figure 6). The CD spectra were obtained at 23 °C, in 10 mM Tris, 100 mM NaF, pH 7.4. Both ri-mel-SH and mel-SH show a double peak at 208 and 222 nm characteristic of α-helix conformation when incubated with saturating concentrations

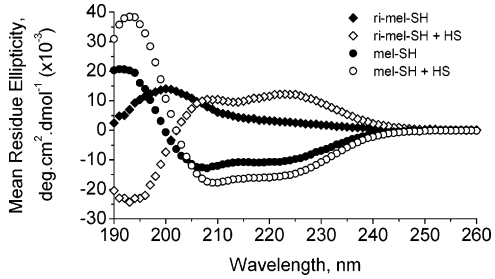

FIGURE 6: CD spectra monitoring conformational changes in analogues of melittin upon saturation with HS. Mean residue ellipticity values of ri-mel-SH (60 μM) in the absence (◆) and presence of 50 μM HS (◇), and mel-SH (60 μM) in the absence (●) and presence of 50 μM HS (○) are plotted as a function of the wavelength. Buffer: 10 mM Tris, 100 mM NaF, pH 7.4.

of HS. The CD spectrum of ri-mel-SH is mirror-imaged at the *x*-axis compared to the conventional α-helix spectrum because ri-mel-SH is composed of all D-amino acids. The helix content calculated with the mean residue ellipticitiy at 222 nm is 32.8 ± 4.4% for ri-mel-SH and 42.9 ± 0.9% for mel-SH. Because ri-mel-SH is predominantly disordered in the absence of HS (random coil content 64 ± 1%, helix content 5.8 ± 2%), this corresponds to approximately a 6-fold increase in the helix content of ri-mel-SH upon binding to HS. Analysis of the CD spectra of mel-SH in the absence of HS reveals a α-helix content of 33.3 ± 3.9%. Binding of HS is also accompanied by an increase of the mel-SH helix content from 33% to 48%, which is, however, smaller than that observed with the retro-inverso analogue.

DISCUSSION

The high transfection activity and low toxicity of melittin conjugates such as dioleoylmelittin (*14*) and melittin-poly(ethyleneimine) (PEI) (*16*) have raised the interest on melittin analogues as potential gene delivery systems. The large positive charge of melittin (+5) suggests that, similarly to cationic lipids (*24*, *25*) and cell penetrating peptides (*26*, *27*), the cellular uptake of melittin and its conjugates is mediated by cell surface HSPG. Despite the numerous studies focusing on the interaction of melittin with lipid membranes (*7*, *31*−*34*), no studies have, to our knowledge, explored the potential involvement of HSPG in the cellular internalization of melittin. In the present work, we address this question by studying the binding equilibrium of two melittin analogues, mel-SH and ri-mel-SH, with heparan sulfate. These peptides can be covalently linked to lipids or cationic polymers via the cysteine residue, which replaces the glycine found in the N-terminus of melittin. The retro-inverso analogue of mel-SH, ri-mel-SH, has the advantage of being stable against protease degradation.

Thermodynamics of HS Binding to Melittin Analogues. The calorimetric data presented here show that HS interacts strongly with both melittin analogues. The binding constants found at 100 mM NaCl and 15 °C for ri-mel-SH and mel-SH are 1.9 × 10^5 M^{-1} and 5.8 × 10^5 M^{-1}, respectively (Table 2), which correspond to dissociation constants in the micromolar range (5−1.5 μM). When compared with TAT and R_9, two cell-penetrating peptides known to depend on HSPG for cellular internalization (*27*, *28*), melittin analogues show similar binding affinities under the same temperature and ionic strength conditions (28 °C, 100 mM, 10 mM Tris, pH 7.4) (Table 3). Replacing the C-terminal cysteine by glycine has almost no influence on the binding parameters at the given conditions (cf. Table 2).

Considering that ∼20% of the residues in melittin and its two analogues are basic amino acids (K and R), we expect electrostatics to be involved in the HS-peptide interaction. This is confirmed by the calorimetric data in two ways. First, binding stoichiometries close to charge neutrality are obtained when the molar ratios are converted to charge ratios. This conversion takes into consideration that (i) each peptide has a net positive charge of +5 and (ii) each HS molecule has an average of ∼55 anionic charges. The latter estimate relies on the sulfur content of HS (6.44%) to determine the number of sulfates and on the assumption that one carboxylate group is present per HS dissacharide (*56*). Following this calculation and based on the molar stoichiometries of ∼14 and ∼15 found for ri-mel-SH and mel-SH, respectively (Table 3), we obtain a charge ratio of ∼1.3 for ri-mel-SH and ∼1.4 for mel-SH. These ratios become closer to charge neutrality if we further assume that the electrostatic binding is limited to the cluster of charged amino acids KRKR (rkrk) located near the N-terminal (C-terminal) of mel-SH (ri-mel-SH). This is a reasonable assumption considering that the additional K is embedded in the hydrophobic part of the peptides, which is supported by the structural data discussed below. With the reduced charge of $z_{el} = 4$, the product of the binding stoichiometry, *n*, with the effective charge, z_{el}, is ∼57 and 62 for mel-SH and ri-mel-SH, respectively (Table 3), leading to a peptide-to-HS charge ratio close to unity for both peptides.

The second evidence for an electrostatic association between HS and melittin analogues is the salt dependency of the binding constants. As commonly observed with electrostatic interactions, the binding affinity of HS to each peptide decreases upon increasing the ionic strength (Table 2). In both cases, the binding constants are linearly related to the NaCl concentration when the data are plotted in a double-logarithmic plot (Figure 5). This behavior is predicted by the polyelectrolyte theory (*46*−*48*), which has been used to analyze the contribution of electrostatics in reactions involving polynucleotides (*49*, *50*) and heparin (*51*−*55*).

The contribution of electrostatics to the overall binding free energy can be estimated from the extrapolated binding constants at 1 M NaCl (*46*, *47*). As opposed to purely ionic interactions, which according to the above model (eqs 1−3) have negligible binding constants at such high salt concentrations (*46*, *47*), the *y*-intercepts of the regressed lines in Figure 5 indicate a significant binding affinity for both peptides at 1 M NaCl; K_T values of ∼1.6 × 10^3 M^{-1} and ∼8.3 × 10^4 M^{-1} are found for ri-mel-SH and mel-SH, respectively. When compared to the binding constants measured at 15 °C and 100 mM NaCl (Table 2), these values suggest that ∼40% and ∼15% of the total free energy of HS binding to ri-mel-SH and mel-SH, respectively, is of electrostatic origin under conditions close to those found in vivo.

An alternative method of estimating the Coulombic component of the HS-melittin analogues interaction is to rely on the calorimetric data of R_9 and TAT (Table 3), two peptides known to interact with HS mainly via electrostatics (*29*, *30*). Assuming that R_9 (TAT) forms a maximum of z_{el} = 9(8) ionic bonds with HS, and defining the interaction as purely ionic, the maximum free energy per ion pair is

Table 3: Thermodynamic Parameters for HS Binding to Cationic Peptides at 28 °C, 10 mM Tris, 100 mM NaCl, pH 7.4[a]

peptide (no. aa)	effective charge (z_{el})	binding stoichiometry (n)	$z_{el} \times n$	K (M^{-1})	ΔH°_{pep} (kcal/mol)	ΔG°_{pep} (kcal/mol)	$T\Delta S^{\circ}_{pep}$ (kcal/mol)	ΔC°_{p} (cal mol/K)
mel-SH[b] (26)	4	14.2 ± 1.9	56.8 ± 7.6	$(6.5\pm 0.8) \times 10^5$	0.5 ± 0.2	-8.0 ± 0.1	8.5 ± 0.2	-322.0
ri-mel-SH[b] (26)	4	15.5 ± 0.7	62.2 ± 2.8	$(4.0 \pm 0.0) \times 10^5$	2.6 ± 0.1	-7.7 ± 0.0	10.3 ± 0.1	-45.0
TAT[c] (11)	8	7.0 ± 0.3	56.0 ± 2.1	$(6.0 \pm 0.6) \times 10^5$	-4.5 ± 0.6	-7.9 ± 0.1	3.4 ± 0.6	135.0
R_9[d] (9)	9	6.9 ± 0.8	62.1 ± 7.2	$(3.1 \pm 0.8) \times 10^6$	-5.5 ± 1.2	-8.9 ± 0.2	3.4 ± 0.1	167.0

[a] Data represent the average ± standard deviation of three measurements. [b] This work. [c] From Ziegler and Seelig, 2004. [d] From Gonçalves et al., 2005.

estimated as $\Delta G_{ion} = \Delta G^{\circ}/z_{el} = -0.99$ kcal/mol (Table 3). Consequently, if we assume that 4 to 5 ionic bonds are formed between HS and each melittin analogue, the corresponding electrostatic contribution to the binding affinity varies between $\Delta G^{\circ}_{el} = -3.96$ kcal/mol and $\Delta G^{\circ}_{el} = -4.96$ kcal/mol. When referenced to the total free energies determined by ITC (Table 3), this corresponds to an electrostatic contribution of ~50−60% for both melittin analogues. These values are higher than those predicted based on the polyelectrolyte theory, and no decision can be made between the two alternatives.

Different energies will contribute to the nonCoulombic part of the interaction energy. An important contribution will come from α-helix formation. Membrane binding studies using amphipathic peptides have demonstrated that membrane-induced α-helix formation is associated with a free energy change of $\Delta G_{helix} \approx -0.2$ to -0.4 kcal/mol per amino acid (*57*−*60*). For ri-mel-SH the helix content increases by about 25% (~6−7 amino acid residues) upon complex formation with HS. Using the experimental results obtained from membrane studies, a total free energy change of −2.6 kcal/mol would be predicted, accounting for 70% of the non-Coulombic energy. In addition, hydrophobic and hydrogen bonding interactions will also make contributions.

Structural Aspects of the HS-melittin Analogues Interaction. Binding of mel-SH and ri-mel-SH to HS produces a conformational change toward a more α-helical structure (Figure 6). Surprisingly, even though the two melittin analogues are much larger than TAT and R_9, about twice as many molecules of mel-SH and ri-mel-SH are bound per HS chain (Table 3). This is possible if the KRKR (rkrk) cluster binds electrostatically to HS and if a major part of the peptide chain extends away from the HS chain. α-helix formation and hydrophobic interactions are usually associated with the release of hydration water, explaining the large entropy increase (Tables 2 and 3) and the negative ΔC°_{p} (Figure 3) observed for the interaction of HS with mel-SH and ri-mel-SH. The heat capacity change for ri-mel-SH ($\Delta C^{\circ}_{p} = -322$ cal mol^{-1} K^{-1}) is much larger than that of mel-SH ($\Delta C^{\circ}_{p} = -45$ cal mol^{-1} K^{-1}) at the same salt concentration. Part of this difference may arise from the more extensive α-helix formation observed for ri-mel-SH upon HS binding. It is also interesting to note that the binding stoichiometry of ri-mel-SH is affected by the salt concentration, increasing from ~13 at low NaCl (≤100 mM) to ~20−25 at higher NaCl concentrations (≥150 mM) (Table 2). The increase in the number of binding sites is accompanied by a distinct decrease in the binding affinity. No such changes are observed with mel-SH (Table 2), suggesting that the binding mode of ri-mel-SH may change depending on the ionic strength. The higher packing density of melittin at high salt concentrations is similar to a condensation phenomenon that has been found for the interaction of cationic peptides with plasmid DNA (*45*).

Comparison with CPPs. TAT and R_9 are two of the best studied cell-penetrating peptides with a cellular uptake known to depend on the expression of cell surface HSPG (*27*, *28*). The TAT peptide (11 amino acids) corresponds to the positively charged protein transduction domain of HIV-1 TAT protein (residues 47−57) and has an electric charge of $z_{el} = 8$ (*61*). The synthetic nonaargine R_9 (9 amino acids) is one of the most efficient CPPs with $z_{el} = 9$ (*62*). Table 3 compares the thermodynamic data obtained with mel-SH, ri-mel-SH, and the two CPPs under similar conditions (28 °C and 100 mM NaCl, 10 mM Tris, pH 7.4). The CPPs are distinctly shorter than the melittin analogues studied here (26 amino acids each), nevertheless, certain similarities are found in their association with HS. First, the product $n \times z_{el}$ of the two CPPs is also close to $z_{el} = 55$, indicating that, similarly to the melittin analogues, the two peptides form complexes with charge ratios close to electroneutrality upon binding to HS. This implies, however, a completely different packing for the two types of molecules, since about twice as many melittin molecules as TAT or R_9 are bound per HS chain (~15 vs ~7). Second, we note that despite the differences in size and charge of the ligands, the binding constants for the interaction with HS are quite similar for the four peptides; K values of $\sim 6 \times 10^5$ M^{-1} are found for TAT and the two melittin analogues, and a slightly higher K of $\sim 3 \times 10^6$ M^{-1} is reported for R_9. As a consequence, the free energies of binding, ΔG°_{pep}, are in the same range for all peptides (Table 3).

On the other hand, it is clear from Table 3 that the origin of the binding free energies is quite different for the four peptides. For mel-SH and ri-mel-SH, the reaction enthalpies are positive and unfavorable for binding and the binding to HS is completely entropy-driven. In contrast, the binding of TAT and R_9 to HS is essentially determined by negative reaction enthalpies, with some entropic contributions. Further differences are revealed by the temperature dependence of the reaction enthalpies; the molar heat capacity changes of mel-SH and ri-mel-SH are negative, those of TAT and R_9 are positive. This clearly indicates that the hydrophobic effect is absent in the HS-CPPs interaction, whereas nonelectrostatic interactions contribute to the formation of the HS-melittin complexes.

Although molecular interpretations of thermodynamic results must be viewed with caution, the results obtained with isothermal titration calorimetry suggest some general differences between the association of melittin analogues (mel-SH and ri-mel-SH) and CPPs (TAT and R_9) with HS. Considering the size of TAT and R_9, and based on the

dominance of electrostatics to the free energy of binding, the CPPs presumably maximize their electrostatic interaction by stretching out along the HS chain. This is also supported by the absence of structural changes in the two peptides upon binding to HS (*29*). In contrast, the much larger size of mel-SH and ri-mel-SH, together with the larger binding stoichiometries require a molecular packing in which the long molecular axis of the peptide molecules extends away from the HS chain. Binding is associated with increased α-helix formation and the HS chain must act as a template for this process. The two melittin analogues are most likely attached electrostatically to the HS polymer via their KRKR (rkrk) clusters, and α-helix formation is an additional driving force for multisite binding.

ACKNOWLEDGMENT

We are grateful to Gabriela Klocek for assistance with the isothermal titration calorimetry measurements of melittin.

REFERENCES

1. Habermann, E. (1972) Bee and wasp venoms, *Science 177*, 314−22.
2. Dempsey, C. E. (1990) The actions of melittin on membranes, *Biochim. Biophys. Acta 1031*, 143−61.
3. Dathe, M., and Wieprecht, T. (1999) Structural features of helical antimicrobial peptides: their potential to modulate activity on model membranes and biological cells, *Biochim. Biophys. Acta 1462*, 71−87.
4. Epand, R. M., and Vogel, H. J. (1999) Diversity of antimicrobial peptides and their mechanisms of action, *Biochim. Biophys. Acta 1462*, 11−28.
5. Kourie, J. I., and Shorthouse, A. A. (2000) Properties of cytotoxic peptide-formed ion channels, *Am. J. Physiol. Cell Physiol. 278*, C1063−87.
6. Vogel, H. (1981) Incorporation of melittin into phosphatidylcholine bilayers. Study of binding and conformational changes, *FEBS Lett. 134*, 37−42.
7. Allende, D., Simon, S. A., and McIntosh, T. J. (2005) Melittin-induced bilayer leakage depends on lipid material properties: evidence for toroidal pores, *Biophys. J. 88*, 1828−37.
8. Quay, S. C., and Condie, C. C. (1983) Conformational studies of aqueous melittin: thermodynamic parameters of the monomer-tetramer self-association reaction, *Biochemistry 22*, 695−700.
9. Hagihara, Y., Kataoka, M., Aimoto, S., and Goto, Y. (1992) Charge repulsion in the conformational stability of melittin, *Biochemistry 31*, 11908−14.
10. Wilcox, W., and Eisenberg, D. (1992) Thermodynamics of melittin tetramerization determined by circular dichroism and implications for protein folding, *Protein Sci. 1*, 641−53.
11. Blondelle, S. E., and Houghten, R. A. (1991) Hemolytic and antimicrobial activities of the twenty-four individual omission analogues of melittin, *Biochemistry 30*, 4671−8.
12. Asthana, N., Yadav, S. P., and Ghosh, J. K. (2004) Dissection of antibacterial and toxic activity of melittin: a leucine zipper motif plays a crucial role in determining its hemolytic activity but not antibacterial activity, *J. Biol. Chem. 279*, 55042−50.
13. Diaz-Achirica, P., Prieto, S., Ubach, J., Andreu, D., Rial, E., and Rivas, L. (1994) Permeabilization of the mitochondrial inner membrane by short cecropin-A-melittin hybrid peptides, *Eur. J. Biochem. 224*, 257−63.
14. Legendre, J. Y., Trzeciak, A., Bohrmann, B., Deuschle, U., Kitas, E., and Supersaxo, A. (1997) Dioleoylmelittin as a novel serum-insensitive reagent for efficient transfection of mammalian cells, *Bioconjugate Chem. 8*, 57−63.
15. Oren, Z., and Shai, Y. (1997) Selective lysis of bacteria but not mammalian cells by diastereomers of melittin: structure−function study, *Biochemistry 36*, 1826−35.
16. Ogris, M., Carlisle, R. C., Bettinger, T., and Seymour, L. W. (2001) Melittin enables efficient vesicular escape and enhanced nuclear access of nonviral gene delivery vectors, *J. Biol. Chem. 276*, 47550−5.
17. Abdallah, B., Hassan, A., Benoist, C., Goula, D., Behr, J. P., and Demeneix, B. A. (1996) A powerful nonviral vector for in vivo gene transfer into the adult mammalian brain: polyethylenimine, *Hum. Gene Ther. 7*, 1947−54.
18. Goula, D., Benoist, C., Mantero, S., Merlo, G., Levi, G., and Demeneix, B. A. (1998) Polyethylenimine-based intravenous delivery of transgenes to mouse lung, *Gene Ther. 5*, 1291−5.
19. Bettinger, T., Carlisle, R. C., Read, M. L., Ogris, M., and Seymour, L. W. (2001) Peptide-mediated RNA delivery: a novel approach for enhanced transfection of primary and post-mitotic cells, *Nucleic Acids Res. 29*, 3882−91.
20. Boeckle, S., Wagner, E., and Ogris, M. (2005) C- versus N-terminally linked melittin-polyethylenimine conjugates: the site of linkage strongly influences activity of DNA polyplexes, *J. Gene Med*.
21. Lasic, D. D. (1997) *Liposomes in gene delivery*, CRC Press, Boca Raton.
22. Yanagishita, M., and Hascall, V. C. (1992) Cell surface heparan sulfate proteoglycans, *J. Biol. Chem. 267*, 9451−4.
23. Lindahl, U., Kusche-Gullberg, M., and Kjellen, L. (1998) Regulated diversity of heparan sulfate, *J. Biol. Chem. 273*, 24979−82.
24. Mounkes, L. C., Zhong, W., Cipres-Palacin, G., Heath, T. D., and Debs, R. J. (1998) Proteoglycans mediate cationic liposome-DNA complex-based gene delivery in vitro and in vivo, *J. Biol. Chem. 273*, 26164−70.
25. Wiethoff, C. M., Smith, J. G., Koe, G. S., and Middaugh, C. R. (2001) The potential role of proteoglycans in cationic lipid-mediated gene delivery. Studies of the interaction of cationic lipid-DNA complexes with model glycosaminoglycans, *J. Biol. Chem. 276*, 32806−13.
26. Rusnati, M., Coltrini, D., Oreste, P., Zoppetti, G., Albini, A., Noonan, D., d'Adda di Fagagna, F., Giacca, M., and Presta, M. (1997) Interaction of HIV-1 Tat protein with heparin. Role of the backbone structure, sulfation, and size, *J. Biol. Chem. 272*, 11313−20.
27. Tyagi, M., Rusnati, M., Presta, M., and Giacca, M. (2001) Internalization of HIV-1 tat requires cell surface heparan sulfate proteoglycans, *J. Biol. Chem. 276*, 3254−61.
28. Fuchs, S. M., and Raines, R. T. (2004) Pathway for polyarginine entry into mammalian cells, *Biochemistry 43*, 2438−44.
29. Ziegler, A., and Seelig, J. (2004) Interaction of the protein transduction domain of HIV-1 TAT with heparan sulfate: binding mechanism and thermodynamic parameters, *Biophys. J. 86*, 254−63.
30. Goncalves, E., Kitas, E., and Seelig, J. (2005) Binding of oligoarginine to membrane lipids and heparan sulfate: structural and thermodynamic characterization of a cell-penetrating peptide, *Biochemistry 44*, 2692−702.
31. Drake, A. F., and Hider, R. C. (1979) The structure of melittin in lipid bilayer membranes, *Biochim. Biophys. Acta 555*, 371−3.
32. Kuchinka, E., and Seelig, J. (1989) Interaction of melittin with phosphatidylcholine membranes. Binding isotherm and lipid headgroup conformation, *Biochemistry 28*, 4216−21.
33. Beschiaschvili, G., and Seelig, J. (1990) Melittin binding to mixed phosphatidylglycerol/phosphatidylcholine membranes, *Biochemistry 29*, 52−8.
34. Ladokhin, A. S., and White, S. H. (2001) 'Detergent-like' permeabilization of anionic lipid vesicles by melittin, *Biochim. Biophys. Acta 1514*, 253−60.
35. Chorev, M., and Goodman, M. (1995) Recent developments in retro peptides and proteins−an ongoing topochemical exploration, *Trends Biotechnol. 13*, 438−45.
36. Fletcher, M. D., and Campbell, M. M. (1998) Partially Modified Retro-Inverso Peptides: Development, Synthesis, and Conformational Behavior, *Chem. Rev. 98*, 763−796.
37. Wiseman, T., Williston, S., Brandts, J. F., and Lin, L. N. (1989) Rapid measurement of binding constants and heats of binding using a new titration calorimeter, *Anal. Biochem. 179*, 131−7.
38. Atherton, E., and Sheppard, R. C. (1989) *Solid-phase peptide synthesis: a practical approach*, IRL Press, Oxford.
39. Fromm, J. R., Hileman, R. E., Caldwell, E. E. O., Weiler, J. M., and Linhardt, R. J. (1997) Pattern and spacing of basic amino acids in heparin binding sites, *Arch. Biochem. Biophys. 343*, 92−100.
40. Cantor, and Shimmel. (1980) in *The behavior of biological macromolecules* pp 849−885, W. H. Freeman and Company, San Francisco.

41. van Holde, K. E., Johnson, W. C., and Ho, P. S. (1998) in *Principles of physical biochemistry* pp 587−637, Upper Saddle River, New Jersey.
42. Reed, J., and Reed, T. A. (1997) A set of constructed type spectra for the practical estimation of peptide secondary structure from circular dichroism, *Anal. Biochem. 254*, 36−40.
43. Seelig, J. (1997) Titration calorimetry of lipid-peptide interactions, *Biochim. Biophys. Acta 1331*, 103−16.
44. Wieprecht, T., and Seelig, J. (2002) *Current Topics in Membranes*, pp 31−56, Elsevier Science, New York.
45. Matulis, D., Rouzina, I., and Bloomfield, V. A. (2000) Thermodynamics of DNA binding and condensation: isothermal titration calorimetry and electrostatic mechanism, *J. Mol. Biol. 296*, 1053−63.
46. Record, M. T., Jr., Lohman, M. L., and De Haseth, P. (1976) Ion effects on ligand-nucleic acid interactions, *J. Mol. Biol. 107*, 145−58.
47. Record, M. T., Jr., Anderson, C. F., and Lohman, T. M. (1978) Thermodynamic analysis of ion effects on the binding and conformational equilibria of proteins and nucleic acids: the roles of ion association or release, screening, and ion effects on water activity, *Q. Rev. Biophys. 11*, 103−78.
48. Manning, G. S. (1978) The molecular theory of polyelectrolyte solutions with applications to the electrostatic properties of polynucleotides, *Q. Rev. Biophys. 11*, 179−246.
49. deHaseth, P. L., Lohman, T. M., and Record, M. T., Jr. (1977) Nonspecific interaction of lac repressor with DNA: an association reaction driven by counterion release, *Biochemistry 16*, 4783−90.
50. Lohman, T. M., deHaseth, P. L., and Record, M. T., Jr. (1980) Pentalysine-deoxyribonucleic acid interactions: a model for the general effects of ion concentrations on the interactions of proteins with nucleic acids, *Biochemistry 19*, 3522−30.
51. Olson, S. T., Halvorson, H. R., and Bjork, I. (1991) Quantitative characterization of the thrombin-heparin interaction. Discrimination between specific and nonspecific binding models, *J. Biol. Chem. 266*, 6342−52.
52. Faller, B., Mely, Y., Gerard, D., and Bieth, J. G. (1992) Heparin-induced conformational change and activation of mucus proteinase inhibitor, *Biochemistry 31*, 8285−90.
53. Thompson, L. D., Pantoliano, M. W., and Springer, B. A. (1994) Energetic characterization of the basic fibroblast growth factor-heparin interaction: identification of the heparin binding domain, *Biochemistry 33*, 3831−40.
54. Mascotti, D. P., and Lohman, T. M. (1995) Thermodynamics of charged oligopeptide-heparin interactions, *Biochemistry 34*, 2908−15.
55. Hileman, R. E., Jennings, R. N., and Linhardt, R. J. (1998) Thermodynamic analysis of the heparin interaction with a basic cyclic peptide using isothermal titration calorimetry, *Biochemistry 37*, 15231−7.
56. Griffin, C. C., Linhardt, R. J., Van Gorp, C. L., Toida, T., Hileman, R. E., Schubert, R. L., II, and Brown, S. E. (1995) Isolation and characterization of heparan sulfate from crude porcine intestinal mucosal peptidoglycan heparin, *Carbohydr. Res. 276*, 183−97.
57. Wieprecht, T., Apostolov, O., Beyermann, M., and Seelig, J. (1999) Thermodynamics of the alpha-helix-coil transition of amphipathic peptides in a membrane environment: implications for the peptide-membrane binding equilibrium, *J. Mol. Biol. 294*, 785−94.
58. Wieprecht, T., Apostolov, O., Beyermann, M., and Seelig, J. (2000) Interaction of a mitochondrial presequence with lipid membranes: role of helix formation for membrane binding and perturbation, *Biochemistry 39*, 15297−305.
59. Ladokhin, A. S., and White, S. H. (1999) Folding of amphipathic alpha-helices on membranes: energetics of helix formation by melittin, *J. Mol. Biol. 285*, 1363−9.
60. Li, Y., Han, X., and Tamm, L. K. (2003) Thermodynamics of fusion peptide-membrane interactions, *Biochemistry 42*, 7245−51.
61. Vives, E., Brodin, P., and Lebleu, B. (1997) A truncated HIV-1 Tat protein basic domain rapidly translocates through the plasma membrane and accumulates in the cell nucleus, *J. Biol. Chem. 272*, 16010−7.
62. Mitchell, D. J., Kim, D. T., Steinman, L., Fathman, C. G., and Rothbard, J. B. (2000) Polyarginine enters cells more efficiently than other polycationic homopolymers, *J. Pept. Res. 56*, 318−25.

BI052221T